Journal of Computational Neuroscience 15, 71–90, 2003

Synchronization of Strongly Coupled Excitatory Neurons: Relating Network Behavior to Biophysics

COREY D. ACKER
Department of Biomedical Engineering, Center for BioDynamics, Boston University, 44 Cummington Street, Boston, MA 02215, USA

NANCY KOPELL
Department of Mathematics, Center for BioDynamics, Boston University, 111 Cummington Street, Boston, MA 02215, USA

JOHN A. WHITE
Department of Biomedical Engineering, Center for BioDynamics, Center for Memory and Brain, Boston University, 44 Cummington Street, Boston, MA 02215, USA
jwhite@bu.edu

Received December 18, 2001; Revised February 12, 2003; Accepted February 19, 2003

Action Editor: John Rinzel

Abstract. Behavior of a network of neurons is closely tied to the properties of the individual neurons. We study this relationship in models of layer II stellate cells (SCs) of the medial entorhinal cortex. SCs are thought to contribute to the mammalian theta rhythm (4–12 Hz), and are notable for the slow ionic conductances that constrain them to fire at rates within this frequency range. We apply "spike time response" (STR) methods, in which the effects of synaptic perturbations on the timing of subsequent spikes are used to predict how these neurons may synchronize at theta frequencies. Predictions from STR methods are verified using network simulations. Slow conductances often make small inputs "effectively large"; we suggest that this is due to reduced attractiveness or stability of the spiking limit cycle. When inputs are (effectively) large, changes in firing times depend nonlinearly on synaptic strength. One consequence of nonlinearity is to make a periodically firing model skip one or more beats, often leading to the elimination of the anti-synchronous state in bistable models. Biologically realistic membrane noise makes such "cycle skipping" more prevalent, and thus can eradicate bistability. Membrane noise also supports "sparse synchrony," a phenomenon in which subthreshold behavior is uncorrelated, but there are brief periods of synchronous spiking.

Keywords: synchrony, phase response, theta rhythm, cycle skipping, membrane noise

1. Introduction

Behaviorally correlated synchronous activity is common in the brain and likely to be functionally important (reviews include O'Keefe, 1993; Farmer, 1998; Gray, 1999; Singer, 1999; Chrobak et al., 2000). Contrary to what many might consider intuitive, such activity is often best mediated by mutual inhibition rather than mutual excitation (e.g., Lytton and Sejnowski, 1991; Wang and Rinzel, 1993; Golomb et al., 1994; White et al., 1998b). This tendency for inhibitory networks to synchronize has been explained mechanistically for

models with relatively simple firing properties (Van Vreeswijk et al., 1994; Hansel et al., 1995; Ermentrout, 1996). Synchrony through mutual excitation can be obtained by changing parameters in simple spiking models (Van Vreeswijk et al., 1994; Hansel et al., 1995; Ermentrout, 1996), but in modeling studies, excitation-based synchronization is often associated with more complex membrane mechanisms, including afterhyperpolarization currents and slow K^+ currents (Crook et al., 1998; Ermentrout et al., 2001).

In this study we are concerned with synchronization mechanisms in the specific context of layer II stellate cells (SCs) of the medial entorhinal cortex (MEC). SCs are responsible for the bulk of the "perforant path" input to the hippocampus. They give rise to extensive axon collaterals within layer II, suggesting that they are coupled in vivo with a significant amount of mutual excitation (Gloor, 1997). Recent physiological studies (Dhillon and Jones, 2000) have failed to find such functional connections in brain slices, either because such monosynaptic connections are rarer than one would suppose from anatomical results, or because the axon collaterals leave the plane of the brain slice. Under intracellular current clamp, SCs are characterized by slow (4–12 Hz) subthreshold oscillations and spike rates (Alonso and Llinás, 1989; Alonso and Klink, 1993). Slow K^+ currents and/or the slow, hyperpolarization-activated cation current I_h are thought to pace theta-frequency activity in SCs (Klink and Alonso, 1993; White et al., 1995, 1998a; Dickson et al., 2000), which is hypothesized to allow mutually coupled SCs to serve as local generators of the 4–12 Hz theta rhythm (Alonso and Llinás, 1989; Alonso and Klink, 1993; White et al., 1995, 1998a; Hasselmo et al., 2000). In this paper, we show in some detail how the properties of the particular slow currents in the stellate cells affect the synchronization behavior of very simple networks with mutual coupling.

Many studies have explored neuronal synchrony using "spike time response" (STR) techniques, which examine network behavior based on how excitatory or inhibitory inputs advance or delay impending spikes (e.g., Kopell, 1988; Ermentrout and Kopell, 1991; Hansel et al., 1995; Ermentrout, 1996; Canavier et al., 1997; Crook et al., 1998; Ermentrout et al., 2001; Winfree, 2001). When the inputs are small, spike advances and delays depend linearly on the size of the perturbation, implying that effects can be calculated analytically from the equations describing the intrinsic currents and the synapses. This "weak coupling" assumption allows mathematically elegant, general, and powerful analysis (e.g. Hansel et al., 1995; Ermentrout and Kopell, 1998; Ermentrout et al., 2001; Neltner and Hansel, 2001), but may give rise to incorrect predictions if the coupling is not adequately small. Even for non-small coupling, techniques based on perturbation-induced changes in spike timing can still be used, with the effects calculated numerically (Jones et al., 2000). In this case, one can still make powerful statements about network behavior based on studies of individual cells. In the present study, we use two STR techniques—one that depends on the weak coupling assumption and one that does not—to study predicted synchronization properties in previously developed models of theta-frequency rhythmicity in SCs (White et al., 1995, 1998a). We validate results from STR methods by comparing them with results from two-cell simulations, and use simple 10-cell simulations to draw more general conclusions. We find that prominent slow potassium currents support synchronization through mutual excitation in modeled SCs, as would be predicted from past studies (Crook et al., 1998; Ermentrout et al., 2001). The slow, hyperpolarization-activated cation current I_h, not studied previously in this context, has similar effects. In models that include slow conductances, we demonstrate that even very small inputs can be "effectively large" (i.e., induced advances or delays that vary nonlinearly with input strength). For large inputs and/or large slow conductances, excitatory inputs can delay subsequent spikes for more than one cycle. In simulations, this phenomenon of cycle skipping tends to promote rapid synchronization. Noise in membrane potential, a prevalent feature in MEC cells (White et al., 1998a, 2000), can amplify the effects of small inputs, increasing the prevalence of cycle skipping and sometimes fundamentally altering the qualitative phase-locked states in which the network can exist. In other parameter regimes, noisy simulated SCs show mostly uncorrelated subthreshold activity, but occasional spontaneous spikes give rise to correlated subthreshold activity, followed by short bouts of synchronized spiking. Portions of this work have been presented in abstract form (Acker et al., 2001).

2. Methods

2.1. Cellular and Network Model

The network formally studied here consists of two mutually coupled model cells, although we also

demonstrate that results from these small networks apply to larger networks. The cellular model is based on measurements from Layer II stellate cells of the MEC (White et al., 1995, 1998a; Dickson et al., 2000; Fransén et al., 2003; equations in Appendix A.1). The single compartment model has a pair of conductances in addition to the standard action potential producing Hodgkin-Huxley sodium and potassium conductances. The additional pair, which allows the cellular model to exhibit sub-threshold oscillations, includes a persistent sodium current I_{Nap} and either a slow, non-inactivating potassium current, I_{Ks} (Eder et al., 1991), or a hyperpolarization-activated, mixed cation current called the h-current or I_{h} (Dickson et al., 2000). In this study we perform all simulations twice, once with I_{h} and again with I_{Ks}. Even though it is possible that a mixture of these currents exists in stellate cells in vivo, the effects of this possibility are not studied here. The cells are always biased to oscillate naturally with a period of 120 ms, corresponding to the period of the theta rhythm in vivo and natural firing frequencies measured in vitro under current clamp (Alonso and Llinás, 1989; Alonso and Klink, 1993). The model cells are connected using model AMPA glutamatergic synapses (Destexhe et al., 1998; equations in Appendix A.2), which are fast and excitatory. Note that by symmetry, since the neuron models are identical, in the two-cell network simulation one can expect both synchrony and anti-synchrony to be solutions of the network. However, these solutions may be stable or unstable and more solutions may also exist.

2.2. *Studying Spike Timing in a Pair of Coupled Cells*

Our methods focus on how fast excitatory interaction affects the difference in spike times between two coupled neurons from one cycle to the next. To do this we use two methods, which we call the *direct* spike time response (STR) method and the *linear* STR method. Details of both are given below. As will be clear shortly, by comparing the predictions of these two methods, one can expose the nonlinear effects of strongly coupled neurons. Application of both the linear and direct STR methods is divided into two steps. We first construct a spike time response curve (STRC), which describes how the timing of the next spike in a periodically firing neuron is affected by a single input. The STRC is very similar to the phase response curve (Hansel et al., 1995; Ermentrout et al., 2001; Kopell and Ermentrout, 2001; Winfree, 2001), but is measured in terms of time instead of phase. The reason for using time instead of phase is that, when the coupling is strong, inputs can have a large effect on the period of the coupled cells, making "phase" ill defined. We then use the STRC to predict the change in spike timing between two mutually coupled neurons from one cycle to the next. This is done by generating the "spike time difference map" (STDM). Given the predictions of network behavior from the STDM, two-cell simulations are always performed to verify their accuracy.

Our STR methods differ from similarly named spike response models (SRMs; Kistler et al., 1997; Gerstner, 2001). See the Discussion for more detail on this issue.

2.2.1. Direct Spike Time Response (STR) Method. The first step in this method is the direct measurement of a STRC (spike time response curve) on a single model neuron; we'll call the result the $\mathrm{STRC}_{\mathrm{dir}}$. The bias current I_{app} is chosen such that the neuron spikes periodically with a desired natural period. A single spike time response is obtained by perturbing the neuron at a certain time in its cycle and measuring the change in its next spike time. The key to this the direct method is that this perturbation is a model AMPA synaptic input (Appendix A.2) and is identical to the input used during network simulations. Keep in mind that this input need not be weak. A $\mathrm{STRC}_{\mathrm{dir}}$ is obtained by varying the perturbation times over the entire cycle, and plotting spike time advance vs. perturbation time (see example STRC, Fig. 1A).

Once the $\mathrm{STRC}_{\mathrm{dir}}$ is computed numerically from a model cell and a model of the synaptic input, one can analytically construct a "spike time difference map" (STDM) for the pair of coupled neurons. This map takes the difference in spike times, Δ, between the cells in one cycle, and computes the difference, $\bar{\Delta}$, in the next cycle. The construction of this map from the $\mathrm{STRC}_{\mathrm{dir}}$ makes two testable assumptions about the network dynamics. The first is the cell that starts in the lead stays in the lead through later cycles. The second assumption is that the timing of each spike is affected by only the most recent presynaptic spike (i.e., the cell's memory does not extend to previous inputs). While in our simulations we never see leader switching, the memory condition requires careful attention. For most of our computations it holds well, but not for all; we will discuss this issue and its implications later in the paper (Fig. 10).

The computation of the STDM from the $\mathrm{STRC}_{\mathrm{dir}}$ is as follows and is illustrated in panel B of Fig. 1.

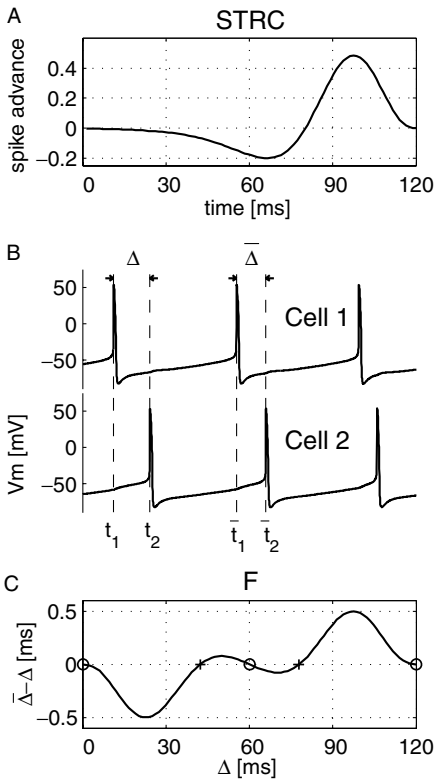

Figure 1. Illustration of STR (spike time response) methods. (A) STRC (spike time response curve). Spike time advance (ms) vs. time of input with respect to previous action potential. Natural period (T) equals 120 ms. (B) Illustration of STDM (spike time difference map) derivation. Given spike times of cell 1 and 2, t_1 and t_2, the next spike times, $\bar{t}_1$ and $\bar{t}_2$, can be predicted using the STRC. (C) $F(\Delta)$ describes the change in STD (spike time difference), $\bar{\Delta} - \Delta$, as a function of Δ, the present STD. Zero crossings with negative slope not less than -2 (open circles) are predicted stable equilibrium STDs. In this illustration, both synchrony and anti-synchrony, STD $= 0$ and 60 ms respectively, are predicted to be stable. Unstable equilibria at 42 and 78 ms (plus symbols) demarcate basins of attraction for the two stable states.

For simplicity we label the STRC_{dir} as P, which is a function of the difference in time between the input and the most recent spike of the postsynaptic cell. Let t_1 and t_2 be the spike times of cell 1 and 2 during some cycle. We choose the labels of cells 1 and 2 such that cell 1 is leading cell 2. Denote by $\bar{t}_1$ and $\bar{t}_2$ the spike times in the next cycle. Then,

$$\bar{t}_1 = t_1 + T - P(t_2 - t_1)$$

That is, the time of firing of cell 1 is the previous time, plus its unperturbed period T, minus the amount of time the next spike is advanced. Similarly,

$$\bar{t}_2 = t_2 + T - P(\bar{t}_1 - t_2).$$

Using $\Delta = t_2 - t_1$ and $\bar{\Delta} = \bar{t}_2 - \bar{t}_1$, we get that

$$\begin{aligned} \bar{\Delta} &= \Delta - P(T - \Delta - P(\Delta)) + P(\Delta) \\ &= \Delta + F_{\text{dir}}(\Delta) \end{aligned} \tag{1}$$

where

$$F_{\text{dir}}(\Delta) = P(\Delta) - P(T - \Delta - P(\Delta)) \tag{2}$$

Equation (1) gives the STDM. $F_{\text{dir}}(\Delta)$ (see example, Fig. 1C) is the amount by which the time difference between the cells changes from cycle to cycle.

From Eq. (1), one can determine equilibrium solutions Δ^0, which describe the time difference between the cells at steady state. We see that Δ^0 is a solution if $F_{\text{dir}}(\Delta^0) = 0$. Requirements for stability of the steady state solution Δ^0 are easily computed in terms of $F_{\text{dir}}(\Delta)$ using theory of one-dimensional maps, which gives us

$$-2 < \frac{d}{d\Delta} F_{\text{dir}}(\Delta)\Big|_{\Delta^0} < 0.$$

Stable solutions are those for which $F_{\text{dir}}(\Delta)$ crosses zero with a slope between -2 and 0 (open circles, Fig. 1C). The "optimal" slope near a zero-crossing is -1, for which the system will converge to equilibrium in one cycle. In general, the closer the slope is to the value -1, the faster the system will converge. Zero crossings with slope outside the interval $(-2, 0)$ indicate the unstable solutions (plus symbols, Fig. 1C) and define boundaries of basins of attraction for the stable states (if there is more than one).

It should be mentioned that in the case of *unidirectional* coupling, $F_{\text{dir}}(\Delta)$ is equivalent to the STRC_{dir}. Therefore, when one cell is driving another at the same firing rate, the zeros and slopes through zero of the STRC_{dir} provide the predictions of network equilibrium behavior.

2.2.2. Linear STR Method. The linear STR method relies on an additional crucial assumption. Delays (or advances) are assumed to be linearly related to size of synaptic input. This assumption is typically accurate only if the actual size of the input is "small" (exactly how small depends on the model cell), so the notion

of weak coupling is therefore tied to linearity. We use the linear method to determine the true weak coupling behavior and compare that to the behavior predicted by the direct method. Because the methods agree exactly in the limit of weak coupling, any observed difference between results is an effect of strong coupling.

Unlike the directly calculated $\mathrm{STRC}_{\mathrm{dir}}$, the linearized STRC, which we'll call the $\mathrm{STRC}_{\mathrm{lin}}$, is computed in two steps. In the first step, a collection of response curves is obtained using extremely brief ($1.0\,\mu$s) pulses of current that can be thought of as approximations to the scaled Dirac δ function. The curves, each called a STRC_{δ}, are obtained using pulses of different amplitude. Pulse amplitude is used to control the amount of charge (area under pulse) delivered by the input. For small (area) inputs, the STRC_{δ} simply scales with (is linearly related to) charge delivered. An infSTRC ("infinitesimal" STRC) can be computed for the neuron in this weak perturbation regime (Hansel et al., 1995). The following limit is evaluated numerically where *Chrg* equals the area under the current pulse and Δ is time of input relative to the previous spike time:

$$\mathrm{infSTRC}(\Delta) = \lim_{Chrg \to 0} \frac{\mathrm{STRC}_{\delta}(\Delta, Chrg)}{Chrg} \qquad (3)$$

This method provides very similar results to the analytical phase response method mentioned in the Introduction. In particular, the infSTRC (Eq. (3)) differs by only by a scaling factor (usually between 1 and 2) from the adjoint computed by XPPAUT (Ermentrout, 2002).

In the second step, infSTRC is then used to analytically obtain a $\mathrm{STRC}_{\mathrm{lin}}$ that predicts the neuron's response to synaptic inputs. This is done by convolving the infSTRC with the PSC (postsynaptic current) that would be elicited by a presynaptic action potential (Hansel et al., 1995). The central idea is that a weak perturbation distributed in time, such as a synaptic potential, can be thought of as a sequential series of essentially instantaneous perturbations weighted properly. The effect on the oscillator's spike time due to the synaptic potential equals the weighted sum of the effects due to each of the instantaneous perturbations. Notice that scaling the coupling strength, which scales the PSCs, simply scales the $\mathrm{STRC}_{\mathrm{lin}}$. Therefore, a response to a strong synaptic input is predicted to be the scaled response to a weaker input.

Once the $\mathrm{STRC}_{\mathrm{lin}}$ is computed via the convolution integral, $F_{\mathrm{lin}}(\Delta)$ is obtained using a simplified version of Eq. (2). This simplification is made to maintain linearity such that scaling the synaptic input, scales $F_{\mathrm{lin}}(\Delta)$ along with the $\mathrm{STRC}_{\mathrm{lin}}$. By expanding the second term in (2) using a Taylor series for small amplitude $P(\Delta)$, where $P(\Delta)$ is the $\mathrm{STRC}_{\mathrm{lin}}$, we find

$$F_{\mathrm{lin}}(\Delta) = P(\Delta) - P(T - \Delta) + E(\Delta) \qquad (4)$$

where

$$E(\Delta) \approx P(\Delta) \cdot P'(T - \Delta). \qquad (5)$$

$E(\Delta)$ is the error in this approximation, which we ignore.

2.3. *Comparison of Predicted and Simulated Network Behavior*

As described above $F(\Delta)$ (from either the direct or linear STR method) gives the predicted dynamics of the two cell network based solely on the STRC from the individual neuron. To confirm the predictions of $F(\Delta)$, we compare them with the behavior of the simulated two-cell network. Details of the two-cell network simulations are given in the next section. There are two ways one could make this comparison. First, one could iterate the STDM (Eq. (1)), predict the spike times of the two cells, plot raster plots of these times, and compare to the spike times found in the two-cell simulation. Rather than this method, we choose the following, which avoids displaying raster plots. From a two-cell simulation, we simply measure the STD (spike time difference, Δ, Fig. 1B) on each cycle. Then, the change in STD, $\bar{\Delta} - \Delta$, can be plotted vs. Δ for each cycle. Simulations with different initial STDs are used to form a complete curve that can be plotted along with $F(\Delta)$ (open circles, Figs. 2–5). Specifying initial STDs for the cells of the network is done using a detailed recording of the state variable waveforms over one full period starting from the beginning of a spike. One cell is always started at time zero at the beginning of a spike. The periodic waveforms for all states are then evaluated at the desired initial STDs to determine the initial conditions of the remaining cells. The same method is used for stochastic simulations except that the state variable corresponding to persistent sodium activation is rounded off so that it represents an integer number of open sodium channels (Appendix A.3).

2.4. Numerical Methods and Simulation Software

Simulation software was written in MATLAB (The MathWorks, Inc.) and C using MATLAB's application program interface (API). Numerical integration was performed in C using a standard adaptive step size Runge-Kutta algorithm (Press et al., 1992), adapted for the MATLAB API, with a relative tolerance of 10^{-6}. The model equations are specified in a separate .c file making it relatively easy to change to a new model and quickly apply the STR methods or run network simulations. Model parameters can be controlled in MATLAB so one can apply the STR methods as a parameter is varied such as we do in this study. For both STRC computation and network simulations, it was necessary to include a threshold crossing detection algorithm because the model AMPA synapse (Appendix A.2) uses a threshold on the presynaptic voltage. A routine based on the secant method of root finding was used (Press et al., 1992) to detect crossing times to within 10^{-4} ms. In several cases, 10-cell simulations with all-to-all coupling (no autapses) were performed along with the two-cell simulations. For these larger simulations, an efficient algorithm (Lytton, 1996) was used that takes full advantage of the simplified synaptic model in order to achieve short simulation times. The maximal synaptic conductance was scaled by $N-1$, where N is the number of cells in the network. Software implementing the linear and direct STR method as well as software for simulation of the two-cell network is available at http://bme.bu.edu/ndl/acker.html with documentation. The programs require MATLAB. XPPAUT, the differential equation utility program (www.pitt.edu/∼phase, Ermentrout, 2002), was used to test the accuracy of our simulations, and to find values of I_{app} required to maintain 120 ms period for uncoupled cells.

2.5. Measuring Limit Cycle Attractiveness

An idea we use later is that of a limit cycle's attractiveness, or how stable it is. Here we describe the measure of limit cycle attractiveness we use, which we label "A". To calculate A, we first use AUTO under XPPAUT to output Floquet multipliers for limit cycles using the command "File/All Info". Behavior of Floquet multipliers and their relation to limit cycle stability and bifurcations is covered in many texts (for example Guckenheimer and Holmes, 1983; Section 11.7, Alligood et al., 1997). For a stable limit cycle, all multipliers lie within the unit circle (they may be complex) except one trivial multiplier that is exactly equal to one. The worst-case multiplier is that which is closest to one in absolute value (not counting the trivial one) and we label that Λ. A is obtained by converting the multiplier Λ to a Floquet exponent, $\sigma = -\ln(\Lambda)/T$, and taking the real part, $A = \text{real}(\sigma)$.

3. Results

3.1. Effects of Coupling Strength

In this section, we show how linear methods of estimating spike time differences begin to fail as coupling strength is increased. With strong coupling, we show that there is another mechanism for synchronization, which we call "cycle skipping". In cycle skipping, starting the two cells near anti-phase leads to suppression of a spike in one of them, such that a sub-threshold oscillation is displayed instead. When the suppressed cell spikes again during the following cycle, its spike time is much closer to that of the non-suppressed cell. The change in network dynamics is substantial and, in some cases, eliminates a stable anti-synchronous state. Cycle skipping can be detected by direct methods, but not linear methods, of calculating the STRC and $F(\Delta)$.

3.1.1. Dynamics in the Model with I_h. We start by illustrating this with the model using I_{h}. Figure 2A demonstrates the effects of coupling strength on STRCs and $F(\Delta)$. The cells are biased so that they spike naturally with a period of 120 ms. In the first row, the maximal synaptic conductance is 0.0006 mS/cm^2. As indicated by the STRCs, the maximal advance induced by this input is approximately 1.7 ms. The directly measured STRC (STRC_{dir}) and linearized STRC (STRC_{lin}) are very similar (closely overlapped), confirming that coupling is weak, according to our operational definition. As expected from the STRCs, $F_{\text{dir}}(\Delta)$ and $F_{\text{lin}}(\Delta)$ in Fig. 2A (right side) are very similar. They predict stable synchrony and unstable anti-synchrony. These predictions are confirmed by results from two-cell simulations (open circles, which represent trajectories of intercellular timing differences for a number of simulations begun with different initial conditions).

After increasing the maximal synaptic conductance by a factor of 10 ($g_{\text{syn}} = 0.006$; Fig. 2A, 2nd row), we begin to observe the effects of strong coupling, as reflected in the fact that the solid and dashed lines no longer match. The negative peak of STRC_{dir} (solid

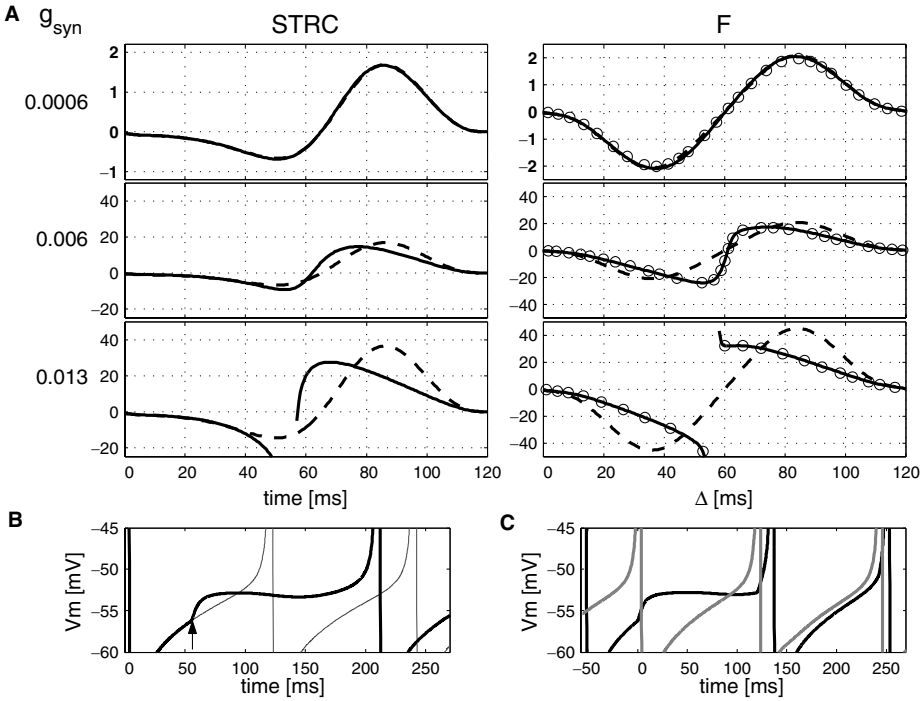

Figure 2. The effects of strong coupling; model includes I_h. (A) g_{syn}, the maximal synaptic conductance or coupling strength (mS/cm^2) is varied among three values as shown on the left. Vertical scale is greatly contracted in the first row to make weak interactions clearly visible. STRCs (spike time advance vs. input time) and $F(\Delta)$s ($\bar{\Delta} - \Delta$ vs. Δ) are shown using both the linearized (dashed lines) and direct method (solid lines). Units are ms. Any difference between these methods indicates an effect of strong coupling. Open circles (right column) are sampled data from two-cell simulations used to verify $F(\Delta)$. Discontinuities in the STRC_{dir} and $F_{\text{dir}}(\Delta)$ indicate cycle skipping, see text. Parameters are given in Appendix A.1 for I_h. (B) Cycle skipping appears while measuring the spike time response to a mid-cycle input. Spikes clipped to show sub-threshold behavior. Two simulations are started from identical initial conditions; in one the cell is left unperturbed (thin gray waveform), while in the other (thick black), an EPSC is applied at the time indicated by the arrow (55 ms). The subsequent spike time in the perturbed waveform is much later than the unperturbed spike and occurs after a sub-threshold oscillation is performed (very small amplitude in this case). Parameters as in row 3 of Fig. 2A. (C) Two cell network simulation with the cells initially 55 ms out of phase. Cycle skipping is seen and the cells are pushed near synchrony in one cycle.

line) is sharper and slightly larger than its linearized counterpart (dashed line). This implies that inputs arriving near mid-cycle can delay the cell slightly more than predicted by scaling its response to weaker inputs. Also, the positive peak falls with a smaller slope. Nonlinearity limits the amount by which the cell can be advanced by inputs arriving just before it was about to spike. The linear method does not sense this natural limit and sometimes predicts anti-causal responses (in response to an input, the cell is advanced such that it spikes before the input).

These two changes in STRC_{dir} shape with $g_{syn} = 0.006$ warp $F_{\text{dir}}(\Delta)$ and therefore change the predicted network dynamics, as seen in the right column of Fig. 2A. These changes can be broken up into two categories: zero crossing locations (and associated slope) that predict locations of stable equilibria, and the shape and amplitude of the curve that predict the evolution, i.e. dynamics, of spike time differences. $F_{\text{dir}}(\Delta)$ and $F_{\text{lin}}(\Delta)$ agree closely on locations of zero crossings, implying that there are no predicted changes in equilibrium behavior due to strong coupling in this case. There are, however, large differences in predicted dynamics. The slope of $F_{\text{dir}}(\Delta)$ near anti-synchrony is much greater than the linearized version. This result implies that if the network is started near anti-synchrony (unstable), it will move away much more rapidly than the linear method predicts. Intercellular time-difference trajectories from 2-cell simulations (open circles) agree closely with predictions from the direct method. The prediction of stable synchrony for $g_{syn} = 0.006$ was verified in 2-cell and 10-cell simulations (data not shown), which showed stable intercellular timing differences of less than 10 μs.

When the maximal synaptic conductance increases to 0.013 mS/cm^2 (Fig. 2A, row 3), the negative peak of the STRC_{dir} "snaps", leaving a gap near 60 ms. This gap is caused by a phenomenon we call "cycle skipping" that is immediately apparent when measuring the spike time response to a mid-cycle input (Fig. 2B). In response to the excitatory perturbation near mid-cycle (arrow, 55 ms), the cell "skips a cycle": rather than spiking, it performs a sub-threshold oscillation (very small amplitude in the I_{h} model), greatly delaying the next spike.

The gap in $F_{\text{dir}}(\Delta)$ is due to the gap in the STRC_{dir}. As a result, $F_{\text{dir}}(\Delta)$ makes the following predictions. If the network is started "in the gap", for example if Δ is initially near 55 ms, cycle skipping is expected, with no prediction of the subsequent dynamics. Otherwise, the network is expected to synchronize without cycle skipping with dynamics given by $F_{\text{dir}}(\Delta)$. The network is not expected to move back into the gap because $F_{\text{dir}}(\Delta)$ is positive to the right and negative to the left of the gap. If Δ is initially greater than 58 ms, it will grow until the cells synchronize. Likewise, if Δ is initially less than 54 ms, it will shrink on subsequent cycles until the cells synchronize.

Two-cell simulations confirm the above predictions and, in addition, allow us to observe the dynamics following cycle skipping (Fig. 2C). When the network is given an initial Δ of 55 ms, cycle skipping takes place as expected and a cell "skips a beat". Typically, when the cell resumes firing it is much closer to being in phase with the other cell (Fig. 2C). When away from anti-synchrony, cycle skipping does not take place and the cells synchronize. Synchrony is therefore the only stable equilibrium state as predicted by the STDM and no persistent behavior including cycle skipping is observed.

3.1.2. Dynamics in the Model with I_{Ks}. Similar results are obtained when the model includes I_{Ks} instead of I_{h}. In this case, the appearance of cycle skipping not only changes network dynamics, it also eliminates one of the stable equilibrium states.

In Fig. 3A, with $g_{\text{syn}} = 0.001$, $F_{\text{dir}}(\Delta)$ and $F_{\text{lin}}(\Delta)$ have an extra pair of maxima and minima compared with the I_{h} case and both synchrony and anti-synchrony are predicted to be stable. When the coupling strength is increased by a factor of 10 ($g_{\text{syn}} = 0.01$), we see something very similar to the I_{h} case. The negative peak of the STRC_{dir} is enlarged, which causes some warping of $F_{\text{dir}}(\Delta)$ (solid line). In particular, the slope of $F_{\text{dir}}(\Delta)$ as it crosses at anti-synchrony is closer to -1, the optimal value for rapid convergence (see Methods). This predicts that if the network starts within the basin of attraction for anti-synchrony, it will anti-synchronize significantly faster than predicted by the linear method.

Notice also for $g_{\text{syn}} = 0.01$ (Fig. 3A, row 2), $F_{\text{dir}}(\Delta)$ does not cross zero at exactly 60 ms, as does $F_{\text{lin}}(\Delta)$. Instead, the zero occurs at approximately 63 ms. Due to the network's symmetry, this implies that when the cells are locked in anti-synchrony, their period is approximately 126 ms, not 120 ms, their uncoupled period. This result agrees well with the STRC_{dir}, which shows that the neurons delay each other by approximately 6 ms on every cycle when in anti-synchrony. Even though a reduced network frequency is not predicted by $F_{\text{lin}}(\Delta)$, the STRC_{lin} predicts that the cells delay each other by approximately 4 ms on every cycle and this corresponds to a coupled period of 124 ms.

When g_{syn} is sufficiently large to cause cycle skipping ($g_{\text{syn}} = 0.015$), we see effects very similar to the I_{h} case. Cycle skipping appears when measuring the spike time response to a mid-cycle input (Fig. 3B) and is the cause of the gap shown in the STRC_{dir} and $F_{\text{dir}}(\Delta)$. Two-cell network simulations (Fig. 3C) reveal cycle-skipping dynamics similar to that with I_{h}. Cycle-skipping tends to push the network away from anti-synchrony and allows the network to quickly synchronize. The stable anti-synchronous solution that is seen if the coupling is sufficiently weak is therefore lost due to cycle-skipping. Previously, albeit under somewhat different circumstances, anti-synchrony has been shown to disappear in the presence of strong coupling (Chow and Kopell, 2000; Kopell et al., 2000).

As in the I_{h} case, additional simulations were performed to confirm predicted equilibria behavior (raw data not shown; intercellular time-difference trajectories shown as open circles in the right column of Fig. 3A). In two-cell simulations anti-synchronization was typically very rapid for initial conditions within the basin of attraction of anti-synchrony. Also, the cells synchronized to within 10 μs after 25 s from an initial STD of 5 ms. There is one interesting effect in Fig. 3A not observed previously with I_{h}. Intercellular time-difference trajectories from two-cell simulations (open circles) do not match the shape of $F_{\text{dir}}(\Delta)$. This discrepancy is due the fact that this cellular model has extended memory: in violation of the assumptions of both direct and linear STR methods, spike timing is determined not only by the most recent input, but also

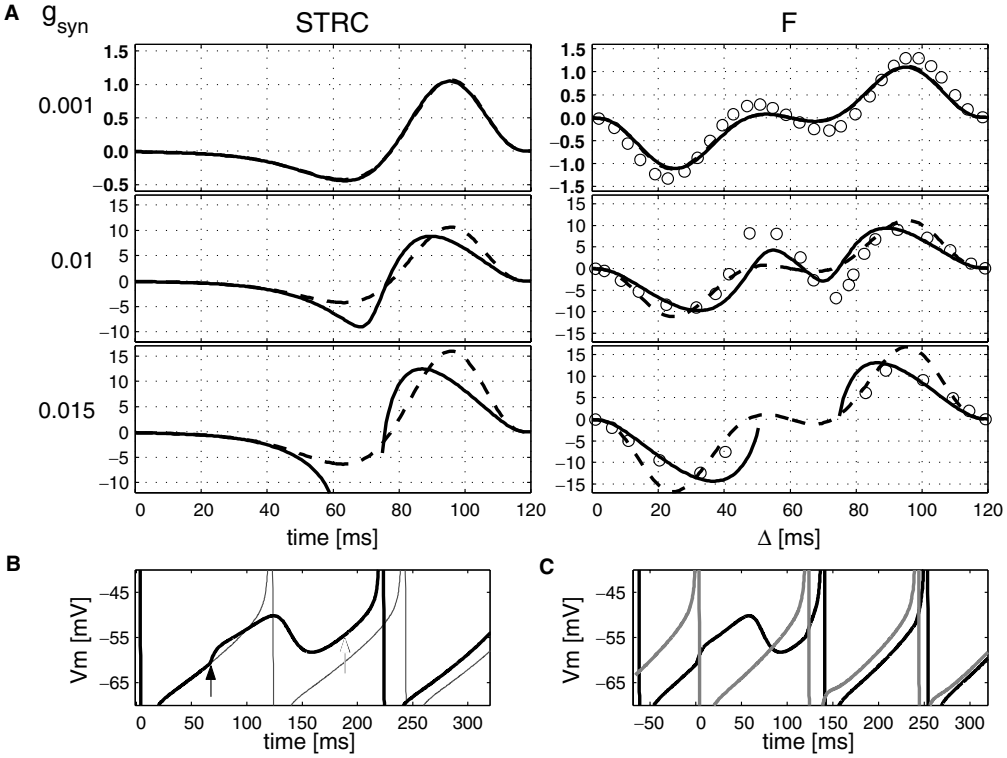

Figure 3. The effects of strong coupling; model includes I_{Ks}. Same format as Fig. 2. (A) Increasing values of g_{syn} are shown on the left. STRCs (spike time advance vs. input time) and $F(\Delta)(\bar{\Delta} - \Delta$ vs. $\Delta)$ are shown using both the linearized (dashed lines) and direct method (solid lines). Units are ms. Open circles plotted along with $F(\Delta)$ are sampled data from two-cell simulations. All parameters are in Appendix A.1 for I_{Ks}. (B) Cycle skipping appears during direct STRC measurement. (C) Two cell network simulation with the cells initially out of phase. Cycle skipping is seen and the cells are pushed near synchrony in one cycle.

by inputs that arrived in previous cycles. This issue is examined further in the Discussion and Fig. 10.

Ten-cell simulations are especially interesting in this case given that the two-cell network is bistable. In general these simulations (data not shown) formed two clusters of cells. Cells within each cluster were closely synchronized and the two clusters of cells fired out of phase with one another. Depending on initial conditions it was possible to create clusters that contained unequal numbers of cells, in which case the two clusters would not fire in exact anti-synchrony. Also, if similar initial conditions were used for all cells, the network would closely synchronize.

3.2. *Changes in Intrinsic Parameters Turn "Weak" Coupling to "Effectively Strong" Coupling and Change Synchronization Properties*

Functionally, "weak" coupling means that there is almost no difference between the linear and direct methods. In this section, we show that this notion of weak coupling depends on intrinsic as well as coupling conductances: if the level of I_h or I_{Ks} is changed, it can change the value of the coupling conductance g_{syn} at which "strong" coupling effects are produced, obtaining them even at very low levels of g_{syn}. Even when there is little difference between the direct and linear method, intrinsic conductances can change the ability to synchronize. This is mirrored in the shape of the STRCs. When the STRC is strictly positive (akin to the "type I" PRC of Hansel et al., 1995), it is not possible to delay the cell with an excitatory input. Cellular models with these properties cannot perfectly synchronize by physiologically realistic mutual excitation (Van Vreeswijk et al., 1994; Hansel et al., 1995; Ermentrout, 1996). By contrast, if the STRC has an initial portion that is negative (akin to the "type II" PRC of Hansel et al., 1995), cells can be either delayed or advanced by excitation, depending on the timing of the input (Figs. 1–3 display type II STRCs). We will show that

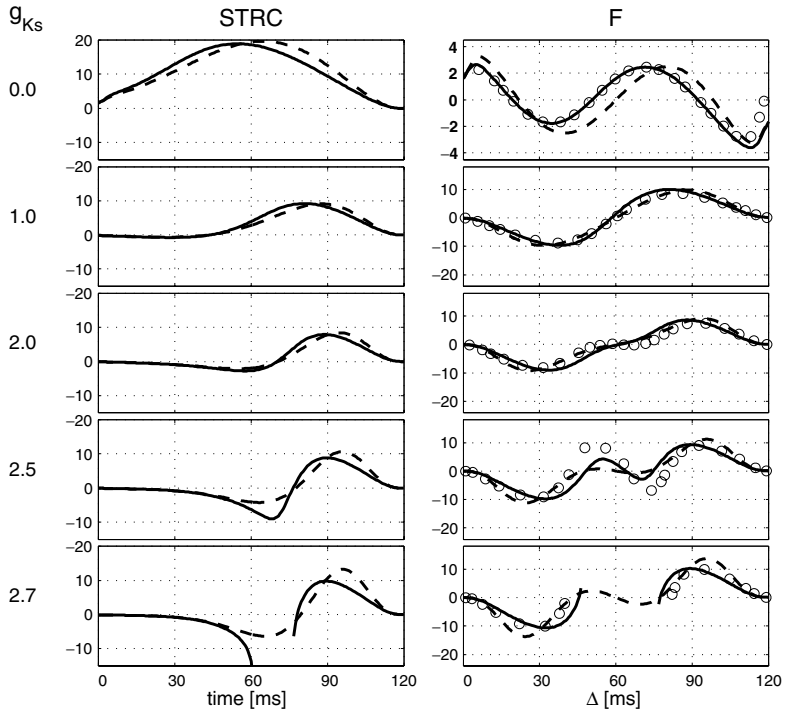

Figure 4. Effects of varying g_{Ks} on network behavior. Five values of g_{Ks} (mS/cm^2), the maximal conductance of I_{Ks}, are shown to the left of the figure. STRCs (spike time advance vs. input time) and $F(\Delta)(\bar{\Delta} - \Delta$ vs. $\Delta)$ are shown using both the linearized (dashed lines) and direct method (solid lines). Units are ms. Open circles are data from two-cell simulations. $g_{\mathrm{syn}} = 0.01$ mS/cm^2. I_{app} is adjusted to maintain a natural period of 120 ms; values for increasing g_{Ks} are: -1.197, 0.191, 1.791, 2.841, and 3.37 μA/cm^2.

changing the level of g_{Ks} or g_{h} can change the STRCs from type I to type II, which changes the synchronization properties of the network.

3.2.1. Effects of Changing g_{Ks}. We start by illustrating this with the model using I_{Ks}. Figure 4 demonstrates the effects of increasing g_{Ks}, the maximal conductance of I_{Ks}, on STRCs and $F(\Delta)$. As g_{Ks} is varied, so too is I_{app}, the bias current, in order to maintain a natural period of 120 ms. G_{syn}, the coupling strength, is maintained at 0.01 mS/cm^2.

3.2.1.1. Increasing g_{Ks} Changes Neurons from Type I to Type II and Creates Bistability. Restricting our attention to the predictions from the linearized STR method (dashed lines), we observe the changes due to increasing g_{Ks} (Fig. 4). With $g_{\mathrm{Ks}} = 0$, so that no slow current exists in the model, the $\mathrm{STRC}_{\mathrm{lin}}$ is strictly positive (type I). From $F_{\mathrm{lin}}(\Delta)$, we see that synchrony is predicted to be unstable, with a stable time lag of 19 ms. When $g_{\mathrm{Ks}} = 1.0$, there is a tiny negative portion early in the $\mathrm{STRC}_{\mathrm{lin}}$. This change in $\mathrm{STRC}_{\mathrm{lin}}$ from type I to type II pushes the stable equilibrium point of $F_{\mathrm{lin}}(\Delta)$ to $\Delta = 0$ ms, indicating synchronous phase-locking. As g_{Ks} is increased from 1.0 to 2.0 mS/cm^2, the negative peak of the $\mathrm{STRC}_{\mathrm{lin}}$ grows in amplitude and shifts to the right (later times in the cycle). $F_{\mathrm{lin}}(\Delta)$ continues to predict that the cells can synchronize using excitation. For $g_{\mathrm{Ks}} > 2.0$, the linear STR method predicts bistability: $F_{\mathrm{lin}}(\Delta)$ crosses zero with negative slope at 60 ms (anti-synchrony) and 0 ms (synchrony).

3.2.1.2. High g_{Ks} Causes Cycle Skipping and Effectively Strong Coupling. For $g_{\mathrm{Ks}} \leq 2$ mS/cm^2, predictions from linear and direct methods are quite similar. However, when $g_{\mathrm{Ks}} = 2.5$ (identical to row 2, Fig. 3) strong coupling effects are very evident. We may say that for this value of g_{Ks}, the value of g_{syn} used in this figure (0.01) is "effectively strong". When g_{Ks} is further increased to 2.7, it seems that the coupling strength is effectively even stronger; the $\mathrm{STRC}_{\mathrm{dir}}$ continues to change shape and cycle skipping is observed. These effects are very similar to those in the last row of Fig. 3A where the synaptic conductance was increased by a factor of 1.5. This apparent increase in coupling strength for large g_{Ks} is due, we suspect, to reduced

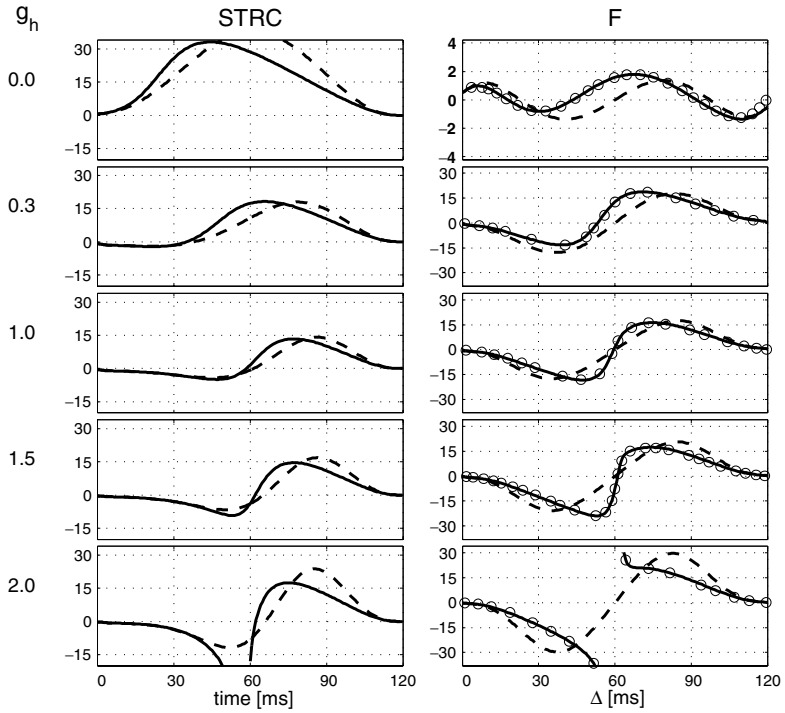

Figure 5. Effects of varying g_{h} on network behavior. I_{h} is included in the model rather than I_{Ks} and the value of g_{h} (mS/cm^2), the maximal conductance of I_{h}, is varied. STRCs (spike time advance vs. input time) and $F(\Delta)(\bar{\Delta} - \Delta$ vs. $\Delta)$ are shown using both the linearized (dashed lines) and direct method (solid lines). Units are ms. Open circles are data from two-cell simulations. $g_{\mathrm{syn}} = 0.006$ mS/cm^2. Values of I_{app} (to maintain a natural period of 120 ms) for increasing g_{h} are: 1.288, 0.618, -1.071, -2.23, and -3.296 μA/cm^2.

attractiveness or stability of the spiking limit cycle. It is possible to measure the attractiveness of a limit cycle (see part E, Methods) and we apply this measure for increasing g_{Ks} in Fig. 9. A discussion of these results is found in part A, Discussion.

3.2.2. Effects of Changing g_h. Similar results are obtained when the model includes I_{h} (Fig. 5). Synchronization properties change as g_{h} is varied. G_{syn}, the maximal synaptic conductance is maintained at 0.006 mS/cm^2.

3.2.2.1. Increasing g_h Changes Neurons from Type I to Type II. Restricting attention to the dashed lines (from the linear method), the following "weak coupling" behavior is observed in Fig. 5. With $g_{\mathrm{h}} = 0.0$, the $\mathrm{STRC}_{\mathrm{lin}}$ is type I and has a very large amplitude. $F_{\mathrm{lin}}(\Delta)$ predicts that a time difference of 22 ms exists between the cells at steady state and that synchrony is unstable. $F_{\mathrm{lin}}(\Delta)$ has a small amplitude compared to the $\mathrm{STRC}_{\mathrm{lin}}$ because the $\mathrm{STRC}_{\mathrm{lin}}$ is nearly symmetric about 60 ms. Consequently, on every cycle the cells advance each other by approximately the same amount, and hence the difference between them changes very little from cycle to cycle. With $g_{\mathrm{h}} = 0.3$, the $\mathrm{STRC}_{\mathrm{lin}}$ changes from type I to type II, and $F_{\mathrm{lin}}(\Delta)$ predicts stable synchrony. In the last three rows, the negative peak of the $\mathrm{STRC}_{\mathrm{lin}}$ grows and moves to the right while $F_{\mathrm{lin}}(\Delta)$ maintains its prediction of stable synchrony and unstable anti-synchrony.

The weakly coupled network does not exhibit bistability as it does with I_{Ks} in the model. This is because the negative peak of the $\mathrm{STRC}_{\mathrm{lin}}$ does not shift sufficiently to the right, as it did with large g_{Ks} (see Discussion for further explanation and proof in Appendix B). It is important to note that the precise location of this negative peak is sensitive to details of I_{h} such as timing and location of its halfway activation point (data not shown). The halfway activation voltage of I_{h} in particular is known to be subject to modulation (Pape, 1996) and this behavior may easily change.

3.2.2.2. Strong Coupling Effects Appear for Different Ranges of g_h and High g_h Causes Cycle Skipping. In

contrast to the case of I_{Ks}, strong coupling effects are seen for large *and* small values of I_h. In row 1 of Fig. 5, the direct STRC has large amplitude and differs significantly from the linearized one. The large amplitude of the $STRC_{dir}$ causes the shift of the unstable equilibrium point near anti-synchrony in $F_{dir}(\Delta)$ from 60 to 45 ms. This leftward shift indicates that the period of the cells decreases when near anti-synchrony to 90 ms (instead of 120 ms). This result agrees well with the $STRC_{dir}$, which indicates that cells advance each other by approximately 30 ms on any cycle in which they are out of phase. For larger values of g_h (rows 2–4), strong coupling effects are still evident. In these cases, strong coupling effects have more dramatic consequences for spike time difference dynamics, discernable from the shape of $F_{dir}(\Delta)$, than for predicted equilibrium time differences, which depend only on behavior of $F_{dir}(\Delta)$ near its zero-crossings.

When $g_h = 1.5$, parameters are identical to row 2 of Fig. 2, and strong coupling effects are noticeable. When g_h is increased to 2.0 (row 5, Fig. 5), dramatic strong coupling effects including cycle skipping appear as they do when the synaptic conductance is significantly increased (row 3, Fig. 2). It appears that this increase in g_h causes an increase in the effective strength of coupling in a similar manner as observed previously with large g_{Ks}. The appearance of cycle skipping in this case has a similar effect on network dynamics: the neurons are pushed away from anti-synchrony and then synchronize quickly. For all values of g_h, $F_{dir}(\Delta)$ (solid lines) and results from simulations (open circles) are in close agreement.

3.3. *How Slow Conductances Can Cause Delays in Response to Excitatory Inputs (Type II STRCs)*

The first rows in Figs. 4 and 5 show that the model stellate cell with no slow current displays a type I STRC, i.e., in response to excitatory input the cell can only be advanced. The rest of Figs. 4 and 5 show that this is not true when there is a slow current that is sufficiently large. Similar results have been reported before (Crook et al., 1998; Ermentrout et al., 2001). In Fig. 6 we explore how the properties of I_{Ks} or I_h, can lead to a type II STRC in which delays are possible that allow the neurons to synchronize via mutual excitation.

In Fig. 6A, m_{Ks}, the activation variable underlying I_{Ks}, is shown in response to an early and a late excitatory input. Any excitatory input tends to activate I_{Ks}, which in turn tends to hyperpolarize the cell. Early inputs

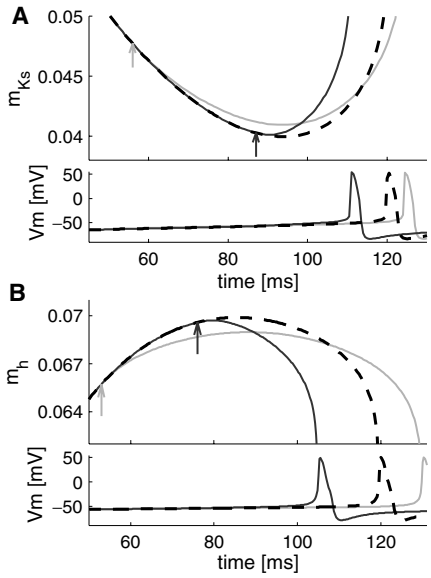

Figure 6. A slow current can cause delays in response to excitatory inputs ("type II" STRC). A, top: Response of m_{Ks} (activation of slow potassium current) to an early (solid gray), and late (solid black) excitatory input. Arrows indicate input times, arrow color matches corresponding trace. Black dashed trace shows unperturbed m_{Ks} trajectory. Bottom shows resulting spike timing. Parameters are as in row 4 of Fig. 4. B: Response of m_h (activation of h-current equals $0.65\ m_{hf} + 0.35\ m_{hs}$), arrows and line types have same meaning as in panel A. Parameters are as in row 4 of Fig. 5.

allow the slow current to activate before the fast sodium channels are recruited and cause the neuron to spike. In this case, the hyperpolarization is sufficient to delay the cell (Fig. 6A, solid gray). In contrast, when inputs arrive late in the cycle, the slow current does not have time to activate before the fast sodium current takes over and the cell spikes before reaching its natural period (Fig. 6A, solid black). Figure 6B demonstrates the same experiment with m_h, the activation of I_h. In general, m_h behaves the same as m_{Ks} except that m_h inactivates in response to excitatory inputs. However, since I_h is an inward current, this also tends to hyperpolarize the neuron. Qualitatively, the results are the same: early inputs delay the next spike, whereas late inputs advance it.

3.4. *Intrinsic Noise Can Promote Synchronous Spiking*

The previous results describe the behavior of a network of deterministically modeled MEC stellate cells. In reality, however, these cells are intrinsically noisy

(White et al., 1998a, 2000). Intrinsic noise has significant effects on experimentally measured STRCs (preliminary data, not shown). In this section we implement a stochastic model of the MEC stellate cell (White et al., 1998a, 2000) and compare network behavior to that obtained previously. Often, the behavior is simply a noisy version of that seen previously and obeys the predictions made by the deterministic STR results. However, for the model MEC neuron (including I_{Ks}) there are two exceptions in which fundamentally different behavior is seen. (1) Cycle skipping-based synchrony (as in Figs. 2C and 3C) occurs for smaller inputs in intrinsically noisy models than in noise-free models. (2) Under conditions of low current drive to noisy model cells or cells in vitro (Alonso and Klink, 1993), cellular behavior is dominated by sub-threshold oscillations and action potentials are generated only sparsely. In this case sub-threshold oscillations control spike timing in a powerful way that promotes "sparse synchronous firing".

3.4.1. Small Inputs Induce Cycle Skipping-Based Synchrony in Noisy Models. Figure 7 demonstrates the consequence of increased input sensitivity due to intrinsic noise. As in the second row of Fig. 3A, the network is bistable: along with synchrony, anti-synchrony is also stable with a wide basin of attraction. This equilibrium behavior is reproduced in Fig. 7A (dashed line). This deterministic behavior is clearly different than the equilibrium behavior observed from the stochastic simulations (solid line, Fig. 7A). The stochastic network displays noisy equilibrium behavior around synchrony only, not around anti-synchrony. Thus the addition of noise has allowed the network to avoid the anti-synchronous state. Figure 7B shows how this is possible. When the deterministic network (top panel, Fig. 7B) is started at anti-synchrony, it remains that way for the duration of the simulation and is therefore locked in anti-synchrony. In contrast, when the stochastic network (bottom panel, Fig. 7B) is started from anti-synchrony, cycle skipping eventually appears and pushes the network close enough to synchrony to allow the network to synchronize. Once synchronized, it remains so.

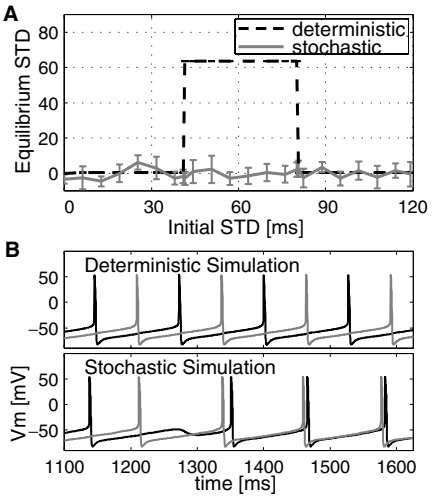

Figure 7. Influence of intrinsic noise on network equilibrium behavior. A: Equilibrium STD (spike time difference) vs. initial STD. For each initial STD, a long two-cell simulation is run and a series of approximately 18 STDs are collected using a measurement window of 4–6 s. The mean and standard deviation of the series of STDs are plotted for each initial STD. Error bars in the deterministic case are not visible while those in the stochastic case represent the steady state effect on STD due to intrinsic noise. Noise eliminates the bistability seen in the deterministic case. B: Deterministic and stochastic simulations both started from anti-synchrony. The deterministic simulation remains locked in anti-synchrony while the stochastic network escapes via cycle skipping and synchronizes. Parameters are in Appendix A.1 for I_{Ks} with $g_{syn} = 0.01$.

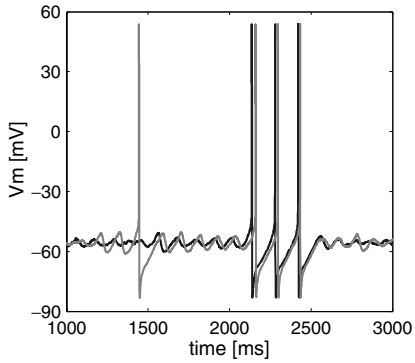

Figure 8. Synchrony among sparse action potentials in simulations including intrinsic noise. Sub-threshold oscillations control spike timing and encourage in-phase spiking. Parameters are in Appendix A.1 for I_{Ks} except $I_{app} = 2.39\ \mu A/cm^2$, $g_{syn} = 0.01$.

3.4.2. Sparse Synchronous Firing. Intrinsic noise can also cause "sparse synchronous firing" (Fig. 8). In this case the two cells predominantly display noisy subthreshold oscillations. Initially, these oscillations are out of phase. The early "rogue" spike ($t = 1400$ ms) in the gray trace fails to elicit a spike in the black, but it does appear to reset the phase of subthreshold oscillations in the black trace, meaning that subsequent noisy oscillations are roughly in phase. Even though the oscillations are quite noisy and not communicated

by the synapses, they sometimes remain in phase for a significant period of time. When the second spike is fired (black trace, $t = 2100$ ms) the postsynaptic cell is significantly depolarized due to the sub-threshold oscillation. A nearly in-phase spike is elicited in the gray trace, initiating a cluster of nearly synchronous activity. The cluster is maintained for two additional cycles by a mixture of these cells' intrinsic tendency to generate spike clusters (Alonso and Klink, 1993; White and Haas, 2001) and the properly phased input each cell receives from its neighbor. Eventually, the spikes fail and noise begins to desynchronize the sub-threshold oscillations. Even if the next random spike fails to elicit a spike, it tends to resynchronize the ensuing oscillations. In this way, sub-threshold oscillations can control spike timing such that clusters of nearly synchronous spike pairs can appear from the noisy background oscillations.

4. Discussion

The behavior of a network of cells is determined by the properties of the participant cells. We find coupling strength, intrinsic voltage-dependent conductances, and the presence of noise all to be important factors in determining the network's behavior. The direct method of estimating spike time response curves (STRCs) and spike time difference maps (STDMs) helps to summarize the cellular properties that are important for network function. Any parameter that significantly changes the shape of the STDM or $F(\Delta)$ also significantly changes the network's behavior. Predictions from direct STDMs are extremely accurate for most cases, in which only the most recent synaptic perturbation has measurable effects on spike timing. Even for cases in which this assumption of "memorylessness" is not met (e.g., Fig. 3; see also below and Fig. 10), results are qualitatively predictive. Results from STR methods and two-cell simulations predict the behavior of larger networks with all-to-all coupling accurately. Synchronization in two-cell networks leads to identical behavior in ten-cell networks. Bistability in two-cell networks leads to two "clusters" (firing synchronously within a cluster and roughly antisynchronously between clusters) in larger networks. The proportion of cells within a given cluster depends on initial conditions.

Our spike time response (STR) methods are very similar to previously developed phase response methods (Hansel et al., 1995; Ermentrout et al., 2001; Kopell and Ermentrout, 2001; Winfree, 2001). However, our direct method avoids the assumption of weak coupling or linearity often made when generating phase response curves (PRCs). This difference allows us to study systems with strong coupling and detect nonlinear effects such as cycle skipping. This gain does not come without a cost: without linear effects of input magnitude on spike timing, one loses all the advantages of linear systems. For the experimentalist, these advantages may be important because they make it possible to predict the STRC for any input given the measurement of a single response curve. Without linearity, it is not possible to predict the exact change in the response curve when the form or size of the input is changed.

Although the direct STR method does require numerical computation of STRCs, it provides considerable insight that is difficult to obtain by only running simulations of the network. For a given set of model parameters, the STR method gives one a map of global network behavior including existence of bistability, domains of attraction, and rates of attraction. Perhaps most importantly, the STR method allows one to easily study the effects of particular membrane conductances on global network behavior.

As mentioned in Methods, STR methods are similar in name to the spike response models (SRMs; Kistler et al., 1997; Gerstner, 2001). In SRMs, one builds kernel-based representations of behavior between spikes, and finds a best-fit threshold value. In practice, only the linear kernel is typically estimated (estimation of higher-order kernels is much more demanding), and the threshold is set to an approximate constant value. Once determined, the SRM can be used to predict the cellular response to an arbitrary, continuous-time input. In our STR methods, one builds functional descriptions of how a periodically-spiking neuron responds to perturbations that occur only once per cycle. For this reason, the STR method outlined here is appropriate only for studying neuronal populations that are entrained at a given firing frequency. By operating under these constrained conditions, the STR method accounts for nonlinear behavior much more easily than do SRM methods. STR analysis could be extended to account for more complex stimulus patterns (e.g., two perturbations per cycle), but at the cost of needing much more data to perform the analysis: the number of data points needed would be expected to be proportional to the square of the number of perturbations per cycle.

4.1. *Effects of Coupling Strength, Intrinsic Conductances, and Noise*

Linear methods of spike time response analysis are predicated on the assumption that perturbation-induced spike time advances and delays are a linear function of the magnitude of the perturbation. Not surprisingly, this assumption breaks down for large enough synaptic conductance perturbations. Here, we see significant breakdown of the assumption of linearity with inputs less than 0.01 mS/cm^2 (with $g_{\mathrm{Ks}} = 2.5$ mS/cm^2). During active exploration and information acquisition, neuronal activity driving stellate cells is likely to be highly coherent (Chrobak et al., 2000), implying that the synaptic "perturbations" received by MEC cells in vivo are large enough to induce considerable nonlinear effects in spike timing, and may be large enough to induce cycle skipping, as seen in Figs. 2C and 3C.

We see two principal effects of increasing magnitudes of the slow conductances g_{Ks} or g_{h}. First, increasing either slow conductance from zero to moderate values changes the STRC from "type I" (always advanced by depolarizing stimuli) to "type II" (delayed for some depolarizing inputs). Correspondingly, $F(\Delta)$ changes to support synchrony via mutual excitation. Second, further increases in g_{Ks} or g_{h} induce "effectively large coupling," in which even a small synaptic perturbation induces nonlinear effects in spike timing, including cycle skipping. The first of these effects is reminiscent of results seen by Ermentrout and colleagues (Crook et al., 1998; Ermentrout et al., 2001). Like (Ermentrout et al., 2001), we see subtly different effects for different slow currents. However, these studies are different in the details; our implementation of I_{Ks} is similar to the M-current I_{M} used by (Ermentrout et al., 2001), but our I_{h} is both quantitatively and qualitatively dissimilar to the spike afterhyperpolarization they studied. More importantly, our work focuses on the effects of large and effectively large inputs, which cannot be studied using their analytical method.

In Figs. 4 and 5, we saw evidence that certain changes in model parameters can cause changes in apparent coupling strength. We suspect that effectively strong coupling is due to a reduction in the "attractiveness", or stability, of the spiking limit cycle. Limit cycle attractiveness is relevant to STR analysis because inputs applied to a nonlinear model with a weakly attractive limit cycle can trigger large divergences from the periodic waveform. Using a measure of attractiveness we call "A" based on the system's worst case Floquet multiplier (see Methods, part E for details), we can investigate this idea. Results are given in Fig. 9, where A is plotted as a function of increasing slow conductance g_{Ks}.

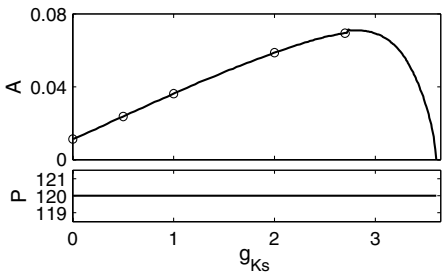

Figure 9. Large values of g_{Ks} lead to reduced limit cycle attractiveness. Top panel shows measure A of limit cycle attractiveness (see Discussion and Methods for details) as a function of increasing slow potassium conductance g_{Ks}. I_{app} is simultaneously varied to maintain a spiking period of 120 ms as indicated in the bottom panel. Specific values of g_{Ks} that correspond to rows of Fig. 4 are indicated by open circles.

In Fig. 9, we see that increasing g_{Ks} eventually leads to a sharp fall off in the limit cycle's attractiveness towards a value of zero. This helps to explain our observations from Fig. 4; the increase in effective coupling strength for large g_{Ks} may be due to a reduction in limit cycle attractiveness. The only discrepancy is that from Fig. 4, effectively strong coupling effects are present when $g_{\mathrm{Ks}} = 2.7$, but we see that the measure of limit cycle attractiveness in Fig. 9 doesn't drop off until immediately after this value. One possible cause of this slight discrepancy is the fact that the measure A only accounts for the system's properties at or very near the limit cycle. Remember that we consider coupling that is not weak and inputs can perturb the system significantly away from the limit cycle where the rate of attraction back to the limit cycle may be less than that right at the limit cycle. For inputs even larger than those considered here, one may expect further reduced accuracy of measure A. In this case it may be necessary to use a different measure of limit cycle attractiveness that takes into account properties of the system in some appropriately large region about the limit cycle.

Whether $F(\Delta)$ predicts stable or unstable anti-synchrony depends on the *location* of the negative peak of the type II STRC: anti-synchrony changes from being unstable to stable when the negative peak shifts to the right past $T_{\mathrm{a}}/2$, where T_{a} is the period of the coupled cells when at anti-synchrony (T_{a} may be different than T, the uncoupled period). In Appendix B

we prove that the change in stability happens when the negative peak is exactly at $T_a/2$. If we look back to the top row of Fig. 3 (I_{Ks}) we see that anti-synchrony is stable and $T_a/2$ equals 60 ms. Given that the negative peak of the STRC is to the *right* of 60 ms we would predict stable anti-synchrony. In the top row of Fig. 2 (I_h), however, the negative peak is to the *left* of 60 ms and anti-synchrony is unstable.

Simulations of coupled noisy neurons can often be understood, at least qualitatively, from noiseless STDMs. Noise in our simulations can amplify the effects of synaptic perturbations. In particular, cycle skipping in response to inputs is more prevalent in noisy simulations than in the noiseless case. This phenomenon effectively destabilizes the anti-synchronous state in our simulations (Fig. 7), converting a bistable deterministic system to a system that hovers around the synchronous state. This effect is seen with noise levels below those observed physiologically (White et al., 1998a). A separate effect was observed in simulations where cycle skipping dominated the cell's natural behavior (Fig. 8). Spikes that appear from this "background" of activity tend to occur in nearly-synchronous clusters.

4.2. *Predictions from both Linear and Direct STR Methods Suffer When Model has Extended Memory*

When the coupling between the cells is truly weak, both the linear and direct STR methods are usually able to accurately predict network behavior. However, this is not always the case, as exemplified by Fig. 3. We believe that this discrepancy is caused by cellular "memory" (i.e., sensitivity to more than just the most recent synaptic perturbation). Figure 10 shows measurements of infSTRCs in response to a single, weak perturbation for two cycles. For the model including I_{Ks} (parameters as in Fig. 3), single perturbations have measurable effects in the second cycle (top panel, dashed line); effects in later cycles (not shown) are negligible. For the comparable model including I_h (Fig. 10, bottom panel), the effects of inputs in the second cycle are minimal. This result likely explains why linear and direct STR methods are more accurate for models with I_h than for models with I_{Ks}.

Inaccuracies due to extended memory could in principle be greatly reduced by developing maps that depend on perturbations during the most recent *two* cycles. Such maps would require measurement of all combinations of delays in perturbations over two firing cycles. Although this is feasible in a model cell, it would be difficult to achieve in the duration of an experimental recording.

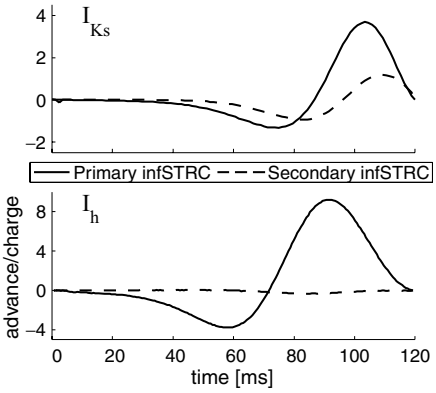

Figure 10. Demonstration of secondary infSTRC. The infSTRC (see Eq. (3)) shows the neuron's response to weak, brief pulses of injected current. For primary infSTRCs (solid lines), advances are measured in the same cycle that the pulse is injected. Secondary infSTRCs (dashed lines) show any residual perturbations in spike timing during the following cycle. In the case of I_h (bottom panel), the secondary infSTRC is essentially zero as the neuron returns to its natural period in the cycle after the perturbation. In the case of I_{Ks} (top panel), the effect of the pulse persists into the second cycle.

4.3. *Future Efforts*

The ability to study strong coupling effects using STR methods represents an important step in developing these methods for more general application in modeling and experimental studies. Future modeling studies should focus on application of STR methods to more realistic conditions, including larger, sparsely coupled networks (Golomb et al., 2001), networks including noise and heterogeneity (Golomb and Rinzel, 1993; White et al., 1998b; Tiesinga and Jose, 2000), and networks that do not fire in a stationary periodic mode. In addition, further work is needed to understand why, after cycle skipping, trajectories return with greater synchrony. Future experimental work should use dynamic clamp technology (Robinson and Kawai, 1993; Sharp et al., 1993; Dorval et al., 2001) to introduce mock synaptic conductances experimentally, and thus directly measure STRCs rather than estimating them using current pulse inputs (Reyes and Fetz, 1993). Routine, successful measurement of STRCs experimentally will require stable whole-cell or perforated

patch recordings that do not significantly change cellular characteristics and are stationary for at least 30 min. Estimation of STDMs from experimental data may require statistical methods to handle jitter in spike timing as well.

Appendix A

A.1. Model MEC Layer II Stellate Cell Equations

The current-balance equation for the modeled neuron is:

$$\begin{aligned} C\frac{dVm}{dt} &= I_{\text{app}} - \left(g_{\text{Na}}m_{\text{Na}}^3 h_{\text{Na}} + g_{\text{Nap}}m_{\text{Nap}}\right)(Vm - V_{\text{Na}}) \\ &\quad - (g_{\text{k}}n^4 + g_{\text{Ks}}m_{\text{Ks}})(V_{\text{m}} - V_{\text{K}}) \\ &\quad - g_{\text{h}}(0.65m_{\text{hf}} + 0.35m_{\text{hs}})(Vm - V_{\text{h}}) \\ &\quad - g_{\text{L}}(Vm - V_{\text{L}}) - g_{\text{syn}}m_{\text{syn}}(Vm - V_{\text{syn}}) \end{aligned} \tag{A.1}$$

where C is membrane capacitance (μF/cm^2), Vm is membrane potential (mV), I_{app} is the applied bias (DC) current (μA/cm^2), g is conductance (mS/cm^2), and units of time are ms. All dynamic variables obey the a first order differential equation expressed either as in Eq. (A.2a), using expressions for the voltage dependent steady state values or (x_∞) and time constants (τ), or as in Eq. (A.2b), in terms of voltage dependent rate constants of α and β.

$$\frac{dx}{dt} = \frac{x_\infty(Vm) - x}{\tau_x(Vm)} \tag{A.2a}$$

$$\frac{dx}{dt} = \alpha_x\,(1 - x) - \beta_x x \tag{A.2b}$$

Definitions for the $\alpha_x(Vm)$ and $\beta_x(Vm)$ functions for each of the dynamic variables are as follows.

$$\alpha_{\text{m Na}}(Vm) = \frac{-0.1 \cdot (Vm + 23)}{\exp(-0.1 \cdot (Vm + 23)) - 1} \tag{A.3a}$$

$$\beta_{\text{m Na}}(Vm) = 4 \cdot \exp\left(\frac{-(Vm + 48)}{18}\right) \tag{A.3b}$$

$$\alpha_{\text{h Na}}(Vm) = 0.07 \cdot \exp\left(\frac{-(Vm + 37)}{20}\right) \tag{A.4a}$$

$$\beta_{\text{h Na}}(Vm) = \frac{1}{\exp(-0.1 \cdot (Vm + 7)) + 1} \tag{A.4b}$$

$$\alpha_{\text{n}}(Vm) = \frac{-0.01 \cdot (Vm + 27)}{\exp(-0.1 \cdot (Vm + 27)) - 1} \tag{A.5a}$$

$$\beta_{\text{n}}(Vm) = 0.125 \cdot \exp\left(\frac{-(Vm + 37)}{80}\right) \tag{A.5b}$$

$$\alpha_{\text{m Nap}}(Vm) = \frac{1}{0.15 \cdot (1 + \exp(-(Vm + 38)/6.5))} \tag{A.6a}$$

$$\beta_{\text{m Nap}}(Vm) = \frac{\exp(-(Vm + 38)/6.5)}{0.15 \cdot (1 + \exp(-(Vm + 38)/6.5))} \tag{A.6b}$$

$$m_{\text{Ks}}(\infty) = \frac{1}{1 + \exp(-(Vm - V_{\text{ha-Ks}})/6.5)} \tag{A.7a}$$

$$\tau_{\text{m Ks}} = 90 \text{ ms} \tag{A.7b}$$

$$m_{\text{hf}_\infty}(Vm) = 1/(1 + \exp((Vm + 79.2)/9.78)) \tag{A.8a}$$

$$\tau_{\text{m hf}}(Vm) = 0.51/[\exp((Vm - 1.7)/10) + \exp(-(Vm + 340)/52)] + 1 \tag{A.8b}$$

$$m_{\text{hs}_\infty}(Vm) = 1/(1 + \exp((Vm + 71.3)/7.9)) \tag{A.9a}$$

$$\tau_{\text{m hs}}(Vm) = 5.6/[\exp((Vm - 1.7)/14) + \exp(-(Vm + 260)/43)] + 1 \tag{A.9b}$$

I_{Ks} and I_{h} are never on simultaneously; i.e. one of g_{h} or g_{Ks} is set to zero. Equations for I_{h} (A.8a)–(9b) are taken from previous studies (Dickson et al., 2000; Fransén et al., 2003) with some simplifying modifications. Simulations were run to confirm that these modifications do not affect results presented in this paper. Parameter values corresponding to Figs. 2 and 3 are as follows. For I_{h} (Fig. 2): $V_{\text{L}} = -65$, $g_{\text{Nap}} = 0.5$, $g_{\text{h}} = 1.5$, $g_{\text{syn}} = 0.006$, $g_{\text{L}} = 0.5$, $I_{\text{app}} = -2.25$. For I_{Ks} (Fig. 3): $V_{\text{L}} = -54$, $g_{\text{Nap}} = 0.21$, $g_{\text{syn}} = 0.01$, $g_{\text{L}} = 0.1$, $I_{\text{app}} = 1.791$, $g_{\text{Ks}} = 2.0$ (default), $V_{\text{ha-Ks}} = -35$. Parameter values that are common to all figures are as follows. $V_{\text{Na}} = 55$, $V_{\text{K}} = -90$, $V_{\text{h}} = -20$, $g_{\text{Na}} = 52$, $g_{\text{k}} = 11$, $C = 1.5$.

A.2. AMPA Synapse Equations and Parameters

A simple, efficient synapse model was implemented (Destexhe et al., 1994) with parameters chosen to mimic the fast kinetics of AMPA receptors (Destexhe et al., 1998). The synaptic gating variable m_{syn}, obeys

the following equation, which depends on neurotransmitter concentration, *NT*.

$$\frac{dm_{\text{syn}}}{dt} = \alpha_{\text{syn}} \cdot NT(1 - m_{\text{syn}}) - \beta_{\text{syn}} m_{\text{syn}} \quad \text{(A.10)}$$

NT depends very simply on the potential of the presynaptic cell as follows. When the presynaptic cell's potential is above a threshold of -20 mV, $NT = 0.001$, otherwise it is zero. In Eq. (A.10), $\alpha_{\text{syn}} = 1100$ and $\beta_{\text{syn}} = 0.19$. For these parameter values, m_{syn} rises in response to a presynaptic action potential to a value near 1 with a time constant of 0.78 ms and then falls with time constant 5.3 ms.

A.3. Stochastic Treatment of Persistent Sodium Channel Population

In the stochastic simulations, the deterministic description of the persistent sodium (I_{Nap}) given above is replaced by a stochastic description used in our past work (White et al., 1998a, 2000) and described briefly here. In the stochastic model, $g_{\text{Nap}} \cdot m_{\text{Nap}}$ is replaced by the ratio $\text{N} \cdot \gamma / \text{SA}$. N is the number of open persistent sodium channels and varies from 0 to 2400 (population size). $\gamma = 20$ pS is the open channel conductance and SA $= 2.29 \times 10^{-4}$ cm^2 is the cell's surface area. This is given by the ratio $\gamma \cdot N / g_{\text{Nap}}$ in order to preserve the maximal conductance of this conductance equal to g_{Nap}. The channels are assumed to be independent and identical. Random numbers are chosen from an exponential distribution based on the equations $\alpha_{\text{Nap}}(Vm)$ and $\beta_{\text{Nap}}(Vm)$ above to determine the time of the next channel transition. The equations are then integrated up to that time using backward Euler integration and the number of open channels is updated. This method is generally used for exact stochastic simulations of chemical reactions (Gillespie, 1977). A maximum step size of 10 μs is enforced; the average time step is approximately 0.5 μs.

Appendix B

Here we show that anti-synchrony is neutrally stable when the negative peak of the type II STRC is located at $T_a/2$, where T_a is the period when the cells are at anti-synchrony. Recall from Methods that the stability of $\Delta = T_a/2$ is given by the derivative of $F(\Delta)$ evaluated at $T_a/2$. We therefore differentiate Eq. (2) in Methods and evaluate at $T_a/2$ in order to determine the stability of anti-synchrony given that the negative peak of the STRC is at $T_a/2$:

$$F'\left(\frac{T_a}{2}\right) = P'\left(\frac{T_a}{2}\right) + P'\left(T - \frac{T_a}{2} - P\left(\frac{T_a}{2}\right)\right) \times \left(1 + P'\left(\frac{T_a}{2}\right)\right) \quad \text{(B.1)}$$

When the negative peak of the STRC is located exactly at $T_a/2$:

$$P'\left(\frac{T_a}{2}\right) = 0$$

Eq. (B.1) can be rewritten:

$$F'\left(\frac{T_a}{2}\right) = P'\left(T - \frac{T_a}{2} - P\left(\frac{T_a}{2}\right)\right). \quad \text{(B.2)}$$

When the cells are perfectly out of phase and have period T_a, on each cycle, the input arriving mid-cycle causes an advance of $T - T_a$. Therefore, T_a is related to T as follows:

$$T_a = T - P\left(\frac{T_a}{2}\right). \quad \text{(B.3)}$$

Subtracting $T_a/2$ from both sides of Eq. (B.3) and plugging into Eq. (B.2), we see that

$$F'\left(\frac{T_a}{2}\right) = P'\left(\frac{T_a}{2}\right) = 0 \quad \text{(B.4)}$$

Equation (B.4) implies that anti-synchrony is neutrally stable when the negative peak of the STRC is exactly at $T_a/2$. A change in stability is therefore expected when the negative peak shifts past $T_a/2$.

Acknowledgments

We are grateful to Jason Ritt, Steve Epstein, Erik Fransén, and John Guckenheimer for helpful discussions, to Bard Ermentrout for assistance with content and XPPAUT, and to fellow members of the NDL lab: Theoden Netoff, Alan Dorval, and Julie Haas. This work was supported by grants from the National Institutes of Health and National Science Foundation (MH 047150 and NSF DMS-9706694 to NK, NS34425 to JAW, and DMS-0109427 to the Center for BioDynamics).

References

Acker CD, Kopell N, White JA (2001) Synchronization of strongly coupled excitatory neurons: Relating biophysics to network behavior. In: Fifth International Conference on Cognitive and Neural Systems. Boston, MA.

Alligood K, Sauer T, Yorke J (1997) Chaos—an introduction to dynamical systems. Springer-Verlag, New York.

Alonso A, Klink R (1993) Differential electroresponsiveness of stellate and pyramidal-like cells of medial entorhinal cortex layer II. J. Neurophysiol. 70: 128–143.

Alonso A, Llinás RR (1989) Subthreshold Na+-dependent theta-like rhythmicity in stellate cells of entorhinal cortex layer II. Nature 342: 175–177.

Canavier CC, Butera RJ, Dror RO, Baxter DA, Clark JW, Byrne JH (1997) Phase response characteristics of model neurons determine which patterns are expressed in a ring circuit model of gait generation. Biological Cybernetics 77: 367–380.

Chow CC, Kopell N (2000) Dynamics of spiking neurons with electrical coupling. Neural Comput. 12: 1643–1678.

Chrobak JJ, Lorincz A, Buzsaki G (2000) Physiological patterns in the hippocampo-entorhinal cortex system. Hippocampus 10: 457–465.

Crook SM, Ermentrout GB, Bower JM (1998) Spike frequency adaptation affects the synchronization properties of networks of cortical oscillations. Neural Comput. 10: 837–854.

Destexhe A, Mainen ZF, Sejnowski TJ (1994) An efficient method for computing synaptic conductances based on a kinetic-model of receptor-binding. Neural Computation 6: 14–18.

Destexhe A, Mainen ZF, Sejnowski TJ (1998) Kinetic models of synaptic transmission. In: C Koch, I Segev, eds. Methods in Neuronal Modeling: From Ions to Networks. MIT Press, Cambridge, MA. pp. 1–26.

Dhillon A, Jones RS (2000) Laminar differences in recurrent excitatory transmission in the rat entorhinal cortex in vitro. Neuroscience 99: 413–422.

Dickson CT, Magistretti J, Shalinsky MH, Fransen E, Hasselmo ME, Alonso A (2000) Properties and role of I(h) in the pacing of subthreshold oscillations in entorhinal cortex layer II neurons. J. Neurophysiol 83: 2562–2579.

Dorval AD, Christini DJ, White JA (2001) Real-time linux dynamic clamp: A fast and flexible way to construct virtual ion channels in living cells. Ann. Biomed. Eng. 29: 897–907.

Eder C, Ficker E, Göndel J, Heinemann U (1991) Outward currents in rat entorhinal cortex stellate cells studied with conventional and perforated patch recordings. Eur. J. Neurosci. 3: 1271–1280.

Ermentrout B (1996) Type I membranes, phase resetting curves, and synchrony. Neural Comput. 8: 979–1001.

Ermentrout B (2002) Simulating, Analyzing, and Animating Dynamical Systems: A Guide to XPPAUT for Researchers and Students, Ist edn. Society for Industrial & Applied Mathematics.

Ermentrout GB, Kopell N (1991) Multiple pulse interactions and averaging in systems of coupled neural oscillators. J. Math. Biol. 29: 195–217.

Ermentrout GB, Kopell N (1998) Fine structure of neural spiking and synchronization in the presence of conduction delays. Proc. Natl. Acad. Sci. USA 95: 1259–1264.

Ermentrout B, Pascal M, Gutkin B (2001) The effects of spike frequency adaptation and negative feedback on the synchronization of neural oscillators. Neural Comput. 13: 1285–1310.

Farmer SF (1998) Rhythmicity, synchronization and binding in human and primate motor systems. J. Physiol. 509: 3–14.

Fransén E, Alonso A, Dickson C, Magistretti J, Hasselmo ME (2003) Ionic mechanisms in the generation of subthreshold oscillations and action potential clustering in entorhinal layer II stellate neurons. Submitted.

Gerstner W (2001) A framework for spiking neuron models: The spike response model. In: F Moss, S Gielen, eds. Neuro-Informatics and Neural Modelling. Elsevier Science B.V. pp. 469–516.

Gillespie DT (1977) Exact stochastic simulation of coupled chemical reactions. Journal of Physical Chemistry 81: 2340–2361.

Gloor P (1997) The Temporal Lobe and Limbic System. Oxford University Press, New York.

Golomb D, Hansel D, Mato G (2001) Mechanisms of synchrony of neural activity in large networks. In: F Moss, S Gielen, eds. Neuro-Informatics and Neural Modelling. Elsevier Science B.V. pp. 469–516.

Golomb D, Rinzel J (1993) Dynamics of globally coupled inhibitory neurons with heterogeneity. Physical Review E Statistical Physics, Plasmas, Fluids, and Related Interdisciplinary Topics 48: 4810–4814.

Golomb D, Wang XJ, Rinzel J (1994) Synchronization properties of spindle oscillations in a thalamic reticular nucleus model. J. Neurophysiol 72: 1109–1126.

Gray CM (1999) The temporal correlation hypothesis of visual feature integration: Still alive and well. Neuron 24: 31–47, 111–125.

Guckenheimer J, Holmes P (1983) Nonlinear oscillations, dynamical systems, and bifurcations of vector fields. Springer-Verlag, New York.

Hansel D, Mato G, Meunier C (1995) Synchrony in excitatory neural networks. Neural Comput. 7: 307–337.

Hasselmo ME, Fransen E, Dickson C, Alonso AA (2000) Computational modeling of entorhinal cortex. Ann. NY Acad. Sci. 911: 418–446.

Jones SR, Pinto DJ, Kaper TJ, Kopell N (2000) Alpha-frequency rhythms desynchronize over long cortical distances: A modeling study. J. Comput. Neurosci. 9: 271–291.

Kistler WM, Gerstner W, van Hemmen LJ (1997) Reduction of Hodgkin-Huxley equations to a single-variable threshold model. Neural Comput. 9: 1015–1045.

Klink R, Alonso A (1993) Ionic mechanisms for the subthreshold oscillations and differential electroresponsiveness of medial entorhinal cortex layer II neurons. J. Neurophysiol. 70: 144–157.

Kopell N (1988) Toward a theory of modelling central pattern generators. In: AH Cohen, S Rossignol, S Grillner, eds. Neural Control of Rhythmic Movements in Vertebrates. Wiley, New York. pp. 369–413.

Kopell N, Ermentrout GB (2001) Mechanisms of phase-locking and frequency control in pairs of coupled neural oscillators. In: B Fiedler, ed. Handbook on Dynamical Systems, Vol. 2, Toward Applications. Elsevier.

Kopell N, Ermentrout GB, Whittington MA, Traub RD (2000) Gamma rhythms and beta rhythms have different synchronization properties. Proc. Natl. Acad. Sci. USA 97: 1867–1872.

Lytton WW (1996) Optimizing synaptic conductance calculation for network simulations. Neural Comput. 8: 501–509.

Lytton WW, Sejnowski TJ (1991) Simulations of cortical pyramidal neurons synchronized by inhibitory interneurons. J. Neurophysiol. 66: 1059–1079.

Neltner L, Hansel D (2001) On synchrony of weakly coupled neurons at low firing rate. Neural Comput. 13: 765–774.

O'Keefe J (1993) Hippocampus, theta, and spatial memory. Curr. Opin. Neurobiol. 3: 917–924.

Pape HC (1996) Queer current and pacemaker: The hyperpolarization-activated cation current in neurons. Annu. Rev. Physiol. 58: 299–327.

Press WH, Teukolsky SA, Vetterling WT, Flannery BP (1992) Numerical Recipes in C: The Art of Scientific Computing, 2nd edn. Cambridge University Press, Cambridge, UK.

Reyes AD, Fetz EE (1993) Two modes of interspike interval shortening by brief transient depolarizations in cat neocortical neurons. J. Neurophysiol. 69: 1661–1672.

Robinson HP, Kawai N (1993) Injection of digitally synthesized synaptic conductance transients to measure the integrative properties of neurons. J. Neurosci. Methods 49: 157–165.

Sharp AA, O'Neil MB, Abbott LF, Marder E (1993) The dynamic clamp: Artificial conductances in biological neurons. Trends Neurosci. 16: 389–394.

Singer W (1999) Neuronal synchrony: A versatile code for the definition of relations? Neuron 24: 49–65, 111–125.

Tiesinga PH, Jose JV (2000) Robust gamma oscillations in networks of inhibitory hippocampal interneurons. Network 11: 1–23.

Van Vreeswijk C, Abbott LF, Ermentrout GB (1994) When inhibition not excitation synchronizes neural firing. J. Comput. Neurosci. 1: 313–321.

Wang XJ, Rinzel J (1993) Spindle rhythmicity in the reticularis thalami nucleus: Synchronization among mutually inhibitory neurons. Neuroscience 53: 899–904.

White JA, Budde T, Kay AR (1995) A bifurcation analysis of neuronal subthreshold oscillations. Biophys. J. 69: 1203–1217.

White JA, Chow CC, Ritt J, Soto-Trevino C, Kopell N (1998b) Synchronization and oscillatory dynamics in heterogeneous, mutually inhibited neurons. J. Comput. Neurosci. 5: 5–16.

White JA, Haas JS (2001) Intrinsic noise from voltage-gated ion channels: Effects on dynamics and reliability in itrinsically oscillatory neurons. In: Moss F, Gielen S, eds. Neuro-Informatics and Neural Modelling. Elsevier Science B.V. pp. 257–278.

White JA, Klink R, Alonso A, Kay AR (1998a) Noise from voltage-gated ion channels may influence neuronal dynamics in the entorhinal cortex. J. Neurophysiol. 80: 262–269.

White JA, Rubinstein JT, Kay AR (2000) Channel noise in neurons. Trends Neurosci. 23: 131–137.

Winfree AT (2001) The geometry of biological time, 2 edn. Springer Verlag, New York.